Hyper-resolution mapping of regional storm surge and tide flooding: Comparison of static and dynamic models.

Jorge A. Ramirez[1*], Michal Lichter[2], Tom J. Coulthard[3], Chris Skinner[3]

[1]Department of Geosciences, Florida Atlantic University, Davie, Florida, USA

[2]Department of Geography, Hebrew University of Jerusalem, Mt. Scopus, Jerusalem, Israel

[3]Department of Geography, Environment, and Earth Sciences, University of Hull, Hull, UK

*Corresponding author (ramirez08063@alumni.itc.nl)

Abstract

Storm tide (combination of storm surge and the astronomical tide) flooding is a natural hazard with significant global social and economic consequences. For this reason, government agencies and stakeholders need storm tide flood maps to determine population and infrastructure at risk to present and future levels of inundation. Computer models of varying complexity are able to produce regional scale storm tide flood maps and current model types are either static or dynamic in their implementation. Static models of storm tide utilize storm tide heights to inundate locations hydrologically connected to the coast, whilst dynamic models simulate physical processes that cause flooding. Static models have been used in regional scale storm tide flood impact assessments but model limitations and coarse spatial resolutions contribute to uncertain impact estimates. Dynamic models are better at estimating flooding and impact but are computationally expensive. In this study we have developed a dynamic reduced-complexity model of storm tide flooding that is computationally efficient and is applied at hyper-resolutions (< 100 m cell size) over regional scales. We test the performance of this dynamic reduced-complexity model and a separate static model at three test sites where storm tide observational data is available. Additionally, we perform a flood impact assessment at each site using the dynamic reduced-complexity and static model outputs. Our results show that static models can overestimate observed flood areas up to 204% and estimate more than twice the number of

people, infrastructure, and agricultural land affected by flooding. Overall we find that that a reduced-complexity dynamic model of storm tide provides more conservative estimates of coastal flooding and impact.

Keywords: storm surge, storm tide, hydrodynamic model, flooding, impact assessment, reduced-complexity

1 Introduction

Globally, storm tide flooding in the past 200 years has claimed the lives of approximately 2.6 million people (Nicholls 2003) and monetary damages from recent storm tide driven floods have repeatedly exceeded $1 billion (Smith and Katz 2013). Storm tide flooding can also be the primary cause of death during a cyclone or hurricane. For example, throughout the United States Atlantic coast 50% of the fatalities related to tropical cyclones were directly caused by storm tide flooding (Rappaport 2014). The combination of projected cyclone intensity and frequency (Emanuel 2013; Grinsted et al 2013) with sea level rise (Stocker et al 2013) and expected population expansion along low lying coastal areas (Curtis and Schneider 2011) will expose more people and infrastructure to storm tide flooding. Particularly vulnerable are coastal regions that are inhabited by low income residents that have limited resources to cope and adapt with extreme flood events (McGranahan et al 2007). A first step towards strengthening resilience in coastal communities requires a robust method for mapping potential regional scale storm tide impact. Regional scale (100-200 km of coastline, 50-100 km inland) impact analysis at hyper-resolution (< 100 m cell size) is needed to provide a synoptic view of population and infrastructure at risk. This information can be used to pinpoint vulnerable locations that require more detailed analysis and local scale efforts (e.g., flood defence structures) to mitigate loses from storm tide flooding.

Key to all storm tide impact analyses is an accurate delineation of storm tide flooding and water depths at flooded locations. Over the past 25 years computer models have offered the possibility to map storm tide flooding at regional scale using models with varying amounts of physical rigour, complexity, and computational efficiency. The simplest method to map storm tide flooding uses a static model, also called the bathtub model. A static storm tide flood model determines flooded locations as those hydraulically connected to the coast and lower than the elevation of the storm tide. Due to the algorithmic simplicity of this model, computational overhead is low and a static model can be used to simply and quickly estimate storm tide flooding and impact over large regions at hyper-resolutions (Hinkel et al 2010; Dasgupta et al 2011; Torresan et al 2012). However, static models do not replicate important characteristics and processes of storm tide flooding. The most important physical processes not accounted for in static models are the: (1) conservation of mass for flows (de Almeida et al 2012), (2) effect of landscape roughness on the spread of floodwater and, (3) attenuation of storm tide by vegetation (Gedan et al 2011). These processes generally limit the extent of storm tide flooding and are needed to replicate flooding in low lying, topographically flat, vegetated regions. Additionally static models assume that flood propagation is only limited by topography and that maximum storm tide water levels are maintained for an infinite duration. The lack of the aforementioned processes and assumptions in static models may be the reason static models consistently overestimate flood extents (Bates et al 2005). Regardless of the physical shortcomings of the static model the computational efficiency of this method has made it a valuable tool to explore scenarios of future storm tide impact (Jongman et al 2012; Mokrech et al 2014; Lloyd et al 2015; Neumann et al 2015), but flood impact derived from statically modelled flood maps may be uncertain in topographically flat regions.

Dynamic models overcome the limitations of the static model by simulating the physical processes related to storm tide flooding. The more complex dynamic models are coupled two-dimensional (2D) or three-dimensional (3D) models that replicate coastal storm tide flooding by simulating atmospheric–ocean–land interactions from the deep ocean to the coast (Forbes et al 2010; Condon and Sheng 2012; Bertin et al 2014) and may include winds, waves, tides, currents, and river runoff. An advantage of coupled models is the ability to map flooding at hyper-resolutions by using unstructured grids that represent the ocean at coarse spatial resolution (1-20 km) and the landscape at fine spatial resolution (5-50 m). This method to partition the model domain increases computational efficiency, but these gains are greatly offset by the act of linking models which increases model complexity and the need to have large model extents to replicate processes (e.g., waves) that occur 100-1000s km offshore. Due to high model complexity and large geographic domains the majority of coupled models are computationally expensive, and require supercomputers with 100-1000s of cores and terabytes of memory (Dietrich et al 2011; Bertin et al 2014) Nevertheless coupled models are useful to replicate historical storm tide events, or a limited number of synthetic events for a single location, but computational overhead hampers their use to investigate storm tide flood impact scenarios requiring many simulations.

Dynamic models of reduced-complexity with simplified physics and lower computational overhead (Larsen et al 2014) have been developed to replicate storm tide flooding (Bates et al 2005; Skinner et al 2015). These 2D models focus on nearshore-land processes that contribute to storm tide flooding, but do not model surge processes in the open ocean. Reduced-complexity models of storm tide inundation have been tested against observed storm tide flood records with good results, but tests have been performed at fine spatial resolution (<50 m) in locations that are smaller in spatial extent than regional scales (Bates et al 2005; Smith et al 2012; Skinner et al 2015). Where these models have been applied on the regional scale, hyper-resolution topographic data has not been used (Bates et al 2005; Lewis et al 2013). Instead, these models have utilized relatively coarse spatial resolution (250-900 m) digital elevation models (DEMs) containing spatially averaged elevations, smoother terrain features and loss of hydrologically important features. As flood model accuracy is highly contingent on the spatial resolution of DEMs (Schumann et al 2014), using these topographically homogenous DEMs will likely produce uncertain flood maps that contain significant error in estimated water depths and flood extents. To date, no regional scale storm tide impact analysis has used flood maps generated from reduced-complexity models, but the computational efficiency of this method demonstrates promise for scenario type modeling.

With the availability of regional scale storm surge water level heights at the coast for the present day (Zervas 2013; Cid et al 2014) and future (Marcos et al 2011) there is a need for a robust method to produce storm tide flood maps at hyper-resolution for use in socio-economic impact analysis. This method should be computationally efficient and contain sufficient physical processes to accurately replicate storm tide hydrodynamics. Here, we present a dynamic model that builds upon recent developments in reduced-complexity modeling of storm tide flooding (Skinner et al 2015), but we apply our model to regional scales at hyper-resolutions. Our model has several distinct advantages over current static and dynamic coupled models of storm tide flooding. Our model is computational efficient and does not require computational resources equivalent to a supercomputer. Furthermore, the flood model is transferable to any coastal location and utilizes datasets that have global spatial extent. These advantages make the model applicable in data poor regions and areas where researchers do not have access to high performance computing facilities. We apply the model at three sites affected by storm tide flooding and test the model by comparing simulated and observed storm tide inundation extents and water height locations. Additionally, we test a static model against the same observed data at the same sites. The results from both model approaches (static and dynamic) are used to determine errors in flood mapping and impact. Overall we find that static models overestimate storm tide flooding and impact, whilst reduced-complexity dynamic models provide more accurate and conservative estimates of flooding and impact.

2 Methods

2.1 Flood modelling

The reduced-complexity dynamic model developed in our study of regional storm tide inundation is largely based on the open source, freely available CAESAR-Lisflood model (Coulthard et al 2013). Within CAESAR-Lisflood the landscape is represented with a DEM and discharge between raster cells is resolved using simplified shallow water equations (Bates et al 2010) rather than the more computationally expensive full shallow water equations. The use of simplified shallow water equations results in a hydrodynamic model that is computational efficient and allows CAESAR-Lisflood to model flooding over regional landscapes (~15,000 km^2) that are represented by hyper-resolution DEMs (< 90 m cell size) with many raster cells (> 1,000,000).

2.1.1 Case Studies

Our dynamic storm tide model was tested at three sites where observed storm tide water levels, flood extent and flood heights were available for direct comparison with model output. The first test site was located in western France near the city of La Rochelle (Figure 1a). This stretch of Atlantic coastline was impacted by wind storm Xynthia on February 27-28, 2010 with maximum wind speeds of 126 km h^{-1}, and the resulting storm surge coincided with a high tide. The second test site selected was the north eastern United States coast near New York City (Figure 1b). On October 29, 2012 hurricane Sandy made landfall in New Jersey, approximately 100 km south of this test site. Although Sandy was only a Saffir-Simpson category 1 hurricane (130 km h^{-1} winds), the storm tide was higher than expected because it coincided with a full moon high tide and a winter storm (Forbes et al 2014). The last test site was located on the southern coast of Myanmar (Figure 1c). On May 2, 2008 cyclone Nargis made landfall on Myanmar as a category 3 cyclone with winds exceeding 178 km h^{-1}. This slow moving cyclone produced a large storm tide that penetrated 50 km inland through the densely populated Irrawaddy delta region (Brakenridge et al 2013). Table 1 summarizes each test site’s physical characteristics, storm tide properties for Xynthia, Sandy, and Nargis and the documented socioeconomic impact from each flood event.

The data requirements for CAESAR-Lisflood are low and to setup a storm tide flood model requires: (1) a DEM to represent the landscape and near shore bathymetry, (2) land cover to assign roughness values to locations within the landscape, and (3) the duration and height of the storm tide. As our intention was to develop a storm tide inundation method that can be applied at any coastal location, we purposely restricted our selection of model input datasets that have global extent. All the spatial datasets for our model were re projected into the spatial projection of World Mollweide to preserve geographic area. For each test site a post processed Space Shuttle Radar Topography Mission (SRTM) DEM (Jarvis et al 2008) at 90 m spatial resolution was obtained (Figure 1). This DEM has a vertical datum of EGM96 and all vertically referenced datasets in our study were transformed into this vertical datum. For dynamic models, preliminary simulations were performed to estimate the maximum spatial extent of inland flooding and DEMs were clipped to encompass the majority of the flooded area. The length of coastline modelled was determined by the spatial extent of the observed flooding and the proximity of the nearest tidal station. Where tidal station data was available (France and USA), coastal locations modelled did not exceed a distance of 70 km from the tidal station. The SRTM DEM used does not represent 'bare earth' and vegetation effects related to SRTM noise (Wilson et al 2007) and canopy heights (Baugh et al 2013) should be considered at locations with dense forest canopy and high vegetation heights. In our study vegetation effects at the USA site were not mitigated because locations near the coast are mostly urban land cover (e.g. New York city). We analysed canopy height data (Simard et al 2011) and found that vegetation heights ≤ 1 m in height covered 69% of the France site and 65% of the Myanmar site. This analysis demonstrates that vegetation effects are less important at these two sites and no changes to the DEM were performed to offset vegetation heights. Global near shore bathymetric data that is commensurate in spatial resolution to the DEM was not readily available. As a proxy for bathymetry a 2.5 km wide seaward shelf was added to the DEM coast with a constant elevation of -5 m. This seaward shelf is the location where the storm tide is added to the model and the shelf elevation was chosen to allow the full range of water levels that occurred in all the test sites. To calculate the flow of water between DEM cells in CAESAR-Lisflood a roughness coefficient (Manning's n) per cell was required. This roughness coefficient determines the resistance a particular land cover imparts on water flow between cells in the DEM. Roughness parameters in CAESAR-Lisflood are generally calibrated until the model replicates observational data like flood extents or water heights (Skinner et al 2015). Although calibration is an important step in dynamic flood simulations (Hunter et al 2007; Stephens et al 2012), observational data of storm tide flooding is rare and independent calibration data was unavailable here, and likely to be unavailable in an operational context. For this reason, we chose to develop an uncalibrated model that instead uses spatially distributed roughness coefficients and typical roughness values for land cover classes. GlobCover 2009 land cover maps (Bontemps et al 2011) were obtained for each site at 300 m spatial resolution. The three sites have characteristically different land cover (Table 1) with west France dominated by croplands, the northeast USA coast primarily urban bounded by inland forest, and south Myanmar mostly croplands interspersed with forest. Manning roughness coefficients for each land cover class were assigned using coefficient values per land cover class reported in Alfieri et al. (2014) (Figure 2).

2.1.2 Storm tide

Strom tide inundation was simulated in the model by gradually raising and lowering storm tide water levels proximate to the coastline over time (Figure 1, ocean area). Observed records of storm tide at tidal stations were used to drive simulations of inundation for wind storm Xynthia at La Pallice, France (Figure 1a) and for hurricane Sandy at Battery Park, USA (Figure 1b). Xynthia water levels were obtained from the REFMAR database (www.refmar.shom.fr) and Sandy water levels from NOAA (http://tidesandcurrents.noaa.gov/). The lack of tide stations in south Myanmar required the use of simulated storm tide for cyclone Nargis (Saito et al 2010; Sayama et al 2012). For each site a water level time series of 62 hrs was extracted at 10 minute time interval for Xynthia and Nargis, and 6 minute time interval for Sandy (Figure 3). These time intervals became the frequency upon which storm tide water levels are updated along the coast within the models. The duration of the time series was chosen to include two tidal peaks prior to the peak storm surge and two tidal peaks afterwards. Operating the model in this manner allows for the development of baseline hydrodynamic conditions for 24 hrs, followed by a period of storm tide flooding of approximately 14 hrs and ample time for drawdown of floodwaters for 24 hrs. At each of our sites rivers hydraulically connected to the ocean were important conduits for storm tide flooding inland. We assumed that average runoff conditions existed in the rivers during the SRTM data collection and river elevations in the DEM represent the water surface. Accordingly we have used a roughness coefficient for water ($n = 0.02$) within river channel locations. As the duration of each simulation was not sufficient for these rivers to form completely, a fixed water elevation of 0.25 m above mean sea level was maintained at river locations for the first 2 hrs of simulation. This water elevation was enough for rivers to develop but not overflow their banks. River locations that correspond to the DEM were determined by using the globally available SRTM water body dataset (https://lta.cr.usgs.gov). Although waves may be included in the observed water levels that drive the models, we do not explicitly reproduce the effect of waves in our simulations. Furthermore in all simulation no soil percolation effects or storm water abatement systems were modeled on land.

Models were executed on a computer with an Intel Xeon E5-2630 processor with 6 cores on 12 simultaneous threads and resulted in wall clock model execution times of 17, 26, and 56 minutes for France, USA, and Myanmar respectively. Model output per test site consisted of a map of maximum flood water heights (DEM elevation + water depth) at each DEM location and this map also delineated the maximum flood extent for a flood event. Additionally, for each test site a static model was performed. Static models of France and USA sites were limited in spatial extent to approximately 50 km inland from the coast, but for Myanmar the inland extent was extended to 100 km inland because this site is a river delta and inundation can reach further inland. The length of coastline modelled per site was the same as the dynamic models. Static models were developed in a geographical information system (GIS, ESRI ArcMap 9.3) by geographically selecting DEM locations that were less than or equal to observed peak storm tide water levels. From this selection of flooded locations, areas that were not hydraulically connected to the coast or rivers connected to the coast were eliminated. The remaining locations represented the maximum flood extent and water heights across the flood extent were equal to the peak storm tide.

2.1.3 Observed flood extent and high water marks

Dynamically and statically modelled flood maps were compared against observed datasets that consisted of flood extents and high water marks (HWM) that represented debris deposited at the flood edge or on the side of structures. For the site in France, a flood extent for wind storm Xynthia consisting of 41 polygons was obtained from satellite images taken 2-4 days after the storm (Breilh et al 2013) and an extensive field survey performed by the French consulting agency SOGREAH (DDTM-17 2011). Additionally maps from the SOGREAH field survey were georeferenced and 388 high water marks were obtained (Figure 4a). For hurricane Sandy a high resolution flood extent in the USA was obtained from the United States Federal Emergency Management Agency Modeling Task Force. This flood extent consisted of 1822 polygons that were created from the interpolation of field verified high water marks. Two hundred nineteen hurricane Sandy high water marks (Figure 4b) were obtained from a post storm survey performed by the United States Geological Survey (McCallum et al 2013). Flood extents for Myanmar Nargis flooding consisted of 772 polygons that were derived from a 250 m spatial resolution MODIS Terra and Aqua imagery (UNOSAT 2008), and 25 high water marks measured by *Fritz et al* (2009). For each test site dynamically and statically derived flood extents were overlaid on their corresponding observed flood extents to determine the total area correctly estimated, underestimated and overestimated. The resulting estimated areas were normalized by the observed flood extent, and presented as percentages. Dynamically and statically modeled maximum flood water heights were compared directly to the water heights at the location of observed high water marks. For both model types vertical error in water heights at each site were calculated as a root mean squared error (RMSE, in m).

2.2 Flood impact assessment

Flood impact assessments for each site were performed to gauge the differences and similarities between impacts derived from observed, static and dynamic flooding. Within this study our intention was to perform a basic impact assessment that reveals how errors in modelling storm tide extent may cascade into an impact assessment. In our assessment we do not provide estimates of economic exposure derived with depth-damage curves, but instead use exposure indicators that include population counts, road networks that represent infrastructure, and agricultural areas. Efforts were made to only use open source data sets that nearly coincided in time with the flood events and regional scale spatial resolutions (< 500 m). Data sets of different sources were used for each test site and for this reason we refrained from performing comparisons between sites. For France gridded population counts for 2009 were obtained from fiscal sources (European Forum for Geography and Statistics 2009). USA population was determined using 2010 census block population counts (U.S. Census Bureau 2010). For Myanmar, a 100 m gridded population model from the WorldPop database was obtained for 2010 with national population counts adjusted to match UN population division estimates (Gaughan et al 2013). All population count datasets were re projected to the World Mollweide equal area projection and converted into population densities (e.g., people per 200 m^2) for each spatial unit of the population count dataset (grid cell or census block). These population density maps were overlaid on the flood extent maps to calculate the total number of people possibly exposed by observed, static and dynamic flooding. Agricultural spatial extent in France was determined from the 2006 Corine land cover map at 100 m spatial resolution (European Environmental Agency 2006), whilst agricultural areas in Myanmar were extracted from 300 m GlobCover 2009 land cover maps (Bontemps et al 2011). At these two sites total agricultural area exposed to storm tide flooding was calculated for observed, static and dynamic flooding. Analysis of agricultural locations exposed to storm tide flooding in the USA was not performed because agricultural land cover is nearly not existent at this mostly urban site. Road network data was obtained for each test site from OpenStreetMap (Haklay and Weber 2008) and overlaid on the flood maps to calculate the total length of roads flooded.

3 Results

3.1 Flood model test

Figure 4 are maps of dynamically modelled maximum water depths (water height – DEM elevation) and flood extents for each storm tide event. Overlaid on these maps are the locations of the HWM where observed water heights were collected. The comparison between HWM with dynamic and static modeled water heights are summarized in Table 2. Comparable vertical error in water heights (RMSE of 1 m) was obtained from both model types (dynamic and static) for the storm tide events in France and the USA. Greater amounts of vertical error in water heights were found for both model types at the Myanmar site. At this site the dynamic model water height RMSE was 2 m, whilst the static model water height difference was 48% greater (2.97 m). The similarities and differences in water height error (observed water height – estimated water height) at all three sites can also be seen in Figure 5. Overall both model types, for all sites, generally underestimated water heights at HWM locations. The performance of dynamic and static models for France and USA was good, with both median vertical errors < 0.5 m. Both model types were less successful in matching HWM in Myanmar. For this site, error in dynamically simulated water heights was less than those obtained with the static model. At this site, the majority of vertical error (interquartile range) in the static model was underestimations in water heights by 2-3.5m, and 1-2 m for the dynamic model.

Table 3 provides a comparison of the observed, dynamic and static flood extents for each test site. For France the dynamic model flooded 79% of the observed flooding that included locations on the near shore islands and land adjacent to the rivers Seudre and Charente (Figure 6a). Overestimations of flooding for the dynamic model were equal to 59% of the observed flooding, with the majority of the overestimations concentrated near the Poitevin marsh and Brouage (Figure 6a). The static model of France correctly flooded 95% of the observed flood areas, but extensive amounts of flooding were estimated where no flooding occurred (Figure 6b). For this site a total of 883 km^2 of land was incorrectly flooded using the static model, and this land area was equal to 204% of the observed flood extent. The greatest amount of error occurred near Charente and Poitevin marsh, where statically modelled flooding occurred 20 km further inland than observed flooding. Dynamic and static flooding of the United States produced comparable results between both model types (Figure 6 c, d). Overall both models underestimated nearly 50% of the observed flooding (Table 3), and performed well at Long Island, but flooding did not advance sufficiently inland at the locations of New York City, Newark, and the inlets of the Raritan bay (Figure 6 c, d). Dynamic flooding of Myanmar produced a good, but conservative mapping of the observed flooding (Figure 6e). The dynamic model correctly estimated 65% of observed flood area, and over- and underestimations of the observed flood area were 33% and 35% respectively (Table 3). All dynamic flooding was near the inland boundary of the observed flooding, and the core of the flooding between Labutta and Bogale was simulated well. A moderate amount of underestimation occurred south west of Pyapon (Figure 6e). The static model correctly estimated a high amount (92%) of the observed flooding, but also flooded a considerable amount of land that was not flooded during this event (Figure 6f). North of Bogale the observed flooding reached 50 km inland, but the static model estimated 90 km of inland flooding that was only limited by the spatial extent of the study area. This area of inland flooding and flooding south of Pyapon contributed to an overestimation of 99% of the observed flood area (Table 3).

3.2 Flood impact assessment

In France population exposed to flooding for observed and dynamically modelled flooding are nearly the same (~20,000 people). Static flooding for France exposed more than double the number of coastal inhabitants (Table 4), and incorrectly exposed 29,000 people to flooding. Observed and dynamically modeled infrastructure flood exposure for France was comparable, but static flooding overestimated infrastructure exposure by 115% (Table 4). Static modelling of France flooded nearly four times the observed agricultural area flooded, whilst the dynamic model only flooded 1.5 times the observed agricultural area. In the USA, both dynamic and static models poorly estimated population exposure. The observed estimate of population exposure for this test site was ~230,000 people, and both static and dynamic models underestimated exposure by 82% and 75% respectively (Table 4). Similarly, infrastructure exposure derived from both model types was approximately half of the observed exposure. In Myanmar, population counts in the static flood extent are roughly twice those in the observed and dynamic flood extents (Table 4). For Myanmar observed and dynamically flooded infrastructure are nearly equivalent, whilst static flood exposure is approximately double the observed infrastructure exposure. The same pattern occurs for Myanmar agricultural impact. Here the dynamic model produces nearly equivalent impact as observed flooding, and the static model floods nearly twice the amount of agricultural land.

4 Discussion

This study has tested the performance of a reduced-complexity dynamic model and static model of storm tide flooding at three sites. Performance of the models was gauged using observed flood water levels and flood extents from storm tide events. In our study we find that static and dynamic models perform similarly regarding flood water levels. For the site in the USA and France both model types produced water levels within 1 m of observed water levels, which is comparable to the performance of dynamic models of greater physical complexity (Forbes et al 2014). At the Myanmar site both model types underestimated flood water levels by 2-3 m. Where both modelling approaches differ is in the spatial extent of flooding. Overall static models have the tendency to significantly overestimate flood extents, whilst the dynamic models produced more conservative flood extents. This is most apparent at the France and Myanmar sites where the static models overestimated 204% and 99% of the observed flood extents respectively. Specifically at the France site the dynamic model significantly reduced the overestimation of flood extents and flooded almost identical locations as a dynamic coupled model of surge, tide and wave flooding (Bertin et al 2014).

Our impact assessment metrics indicated that at France and Myanmar our dynamic model nearly produced the same amount of socio-economic impact that the observed flood extent estimated. This contrasted with static storm tide flooding that resulted in highly inflated socio-economic impact at the same test sites. These results suggest that static models at least estimated twice the amount of impact than dynamic models with the difference caused by the overestimation of flood extents. This demonstrates that static models that do not consider landscape roughness or flood hydrodynamics can produce high overestimates of flood impact. Both model types underestimated impact at the USA site, and this was mostly caused by insufficient flooding.

Differences between observed and modelled flood extents in both model types may be the result of limitations on model inputs and quality of spatial data. In our study we used storm tide water levels recorded at one geographic location, even though storm tide heights can vary along the coast according to the physical structure of a storm and differences in bathymetry. Not accounting for geographic variability in strom tide heights may explain the underestimation of hurricane Sandy's flood extent by both model types. Evidence for this is provided by a network of inland storm tide sensors (McCallum et al 2013) that measured peak storm tide heights at locations throughout the USA site during Sandy. This data indicates that peak storm tide can be 1-2 m greater at sites 40 km from the tidal gauge station (Battery Park) used in our flood model. If more tidal gauge stations were available for our test sites it would have been possible to partition the coast into segments (Lewis et al 2013) and account for spatial heterogeneity in storm tide heights within both model types. We also suggest that care is taken when selecting tidal station data, as bathymetric effects at station locations can amplify or attenuate storm tide. When possible metadata (e.g. bathymetry) should be obtained for tidal stations and used to determine records that are not significantly affected by relatively shallow locations or steeply sloping sea beds. Where tidal station data is not available or of poor quality our reduced-complexity flood model can optionally be driven with modelled storm surge heights applied to coastal segments with similar surge characteristics (Lewis et al 2013).

A secondary reason for mismatches between observed and modelled flood extents may be the result of feature representation within the DEM. Schumann et al (2014) showed that DEM resolution and quality can have a significant impact upon the outcome and calibration of flood inundation models like CAESAR-Lisflood. At the France site the spatial coarseness (90 m) of the DEM has 'smoothed' the heights of flood defence features (natural barriers and sea walls) and this has contributed to flood extent overestimation by both model types. Finer spatial resolution DEMs with global coverage could not be obtained at the time this study was performed, but now 30 m SRTM DEMs have been released and this spatial resolution may better represent flood defences. Where LIDAR (Light Detection And Ranging) DEMs exist at fine spatial resolution (1-2 m) elevations of flood defences can be extracted and directly added to a regional scale DEM. Likewise, locations and heights of flood defences can be obtained from local agencies and this information can be incorporated into the DEM. Another approach is to use subgrid parameterization methods to embed fine scale flood defence features within a coarser scale grid (Yu and Lane 2006; McMillan and Brasington 2007). Subgrid parameterization methods have been implemented in a modified Lisflood-FP as a grid-by-grid ‘porosity’ parameter that represents the blocking effect of microtopography (McMillan and Brasington 2007). Although these methods have not been developed in CAESAR-Lisflood, such an implementation is possible and could be used to represent coastal flood defences within regional scale DEMs. This improvement of feature representation in DEMs could be used to test different flood defence schemes with CAESAR-Lisflood and help select schemes that offer optimal flood protection.

Additional simulations for each site were carried out to test the effects of bathymetry on storm tide flooding. Adding the 30 arc second spatial resolution GEBCO bathymetry (Weatherall et al 2015) to the DEM produced very small differences in maximum flood extents and water depths. Bathymetry should be included in the reduced-complexity model if the storm tide was introduced at an offshore location and propagated towards the coast. If this were the case, near shore slopes and elevations would have an effect on the storm tide and inland flooding. Instead we have introduced the storm tide uniformly across the near shore area and this does not allow bathymetry to have an effect on the storm tide. This finding suggests that high resolution bathymetry is not required to achieve good performance with the reduced-complexity model and storm tide flooding can still be reasonably estimated where bathymetric data is not available or of poor quality.

The underestimation of water heights at the Myanmar site may also be due to the role of waves. At this site no records exist for cyclone Nargis storm tide heights but post storm HWM suggested that the storm tide was 5 m with 2 m waves superimposed on the storm tide (Fritz et al 2009). Our dynamic and static models attained a peak storm tide near 7 m, which is equivalent to the combined surge, tide and waves, but neither model type explicitly replicated the effects of waves and this may explain the underestimation of flood water levels at this site. The overall poor performance of static models is largely due to their failure to represent hydrodynamic processes or conservation of mass. Therefore static models will not incorporate the effect of landscape roughness slowing the spread of floodwater or a flood wave. As such, the lateral movement of flooding in static models was only limited by topography (in this case DEM elevation) leading to an overestimation of flood extent especially in the low elevation France and Myanmar sites. At these sites landscape roughness was represented in the dynamic models and better model performance could be attributed to the land cover providing sufficient resistance to flow thus affecting the speed and spatial limit of the flood wave advance. Such findings support previous research by Gedan et al.

(2011) and de Almeida et al. (2012) and importantly show that hydrodynamic and landscape roughness effects are also important at the hyper-resolution scale.

Our study has not investigated the influence of uncertainty within the data and modelling process on the simulated storm tide flooding. Model uncertainty analysis requires multiple model runs (100-1000s) with each model run having random values chosen for uncertain parameters and the resulting model outputs summarized into probabilistic flood estimates (Skinner et al 2015). For example, Stephens et al. (2012) demonstrated how a Monte Carlo based approach applied to model parameters, including roughness values, could be used to produce probabilistic flood extents, which are more useful for determining flood risk and impact in an operational setting. Given that uncertainty analysis requires many model runs, this analysis is more feasible with models that are computationally efficient and produce model output quickly. For this reason, our reduced-complexity storm tide model is more suited for uncertainty analysis than storm tide models that are computationally expensive and time-consuming.

5 Conclusions

Our findings show that a simple hyper-resolution dynamic reduced-complexity model of storm tide flooding can replicate flood water heights, flood extent, and provides socio-economic impact at regional scale. Our model is the first implementation of a reduced-complexity storm tide inundation model at a fine spatial resolution (90 m) and regional scale. Our approach to estimate flood impact is based on an open source model that is computationally efficient, does not require model calibration, can be operated with limited training, and was developed with freely available data of global extent. The approach is transferable to any location in the world and is a valuable tool for flood risk management in poorer coastal regions with sparse data and limited computational resources. Most importantly our approach could be used to estimate future coastal flooding and impact with storm tide scenarios of different return periods and sea levels. Additionally, future work with both model types (static and dynamic) could determine whether the uncertainty within the forcing water-level boundary condition (e.g. spatial or temporal variability of water-levels (Lewis et al 2011; Quinn et al 2014)) is larger than the difference between inundation modelling methods. Another follow up study with both model types could gauge the role of DEM resolution on the flood results (Savage et al 2015) and socioeconomic impact. A study like this would determine at which spatial resolution does model performance deteriorate and identify when hyper-resolutions DEMs are needed.

Dynamic reduced complexity models therefore offer a more conservative yet easily implementable alternative to existing methods. The primary advantage our dynamic model offers over static models is the inclusion of landscape roughness effects on flooding. Importantly, we find that static models of storm flooding applied in topographically flat regions are highly erroneous and this contributes to exaggerated socio-economic impact assessments. We recommend that regional storm tide impact in topographically flat regions always utilize dynamic models that consider landscape roughness.

6 Acknowledgements

The authors wish to thank the two anonymous reviewers. CAESAR-Lisflood is available from http://sourceforge.net/projects/caesar-lisflood/ and the source code for the modified version of CAESAR-Lisflood used in this study can be obtained from Jorge Ramirez.

7 References

Aerts JCJH, Lin N, Botzen W, et al (2013) Low-Probability Flood Risk Modeling for New York City. Risk Anal 33:772–788. doi: 10.1111/risa.12008

Alfieri L, Salamon P, Bianchi A, et al (2014) Advances in pan-European flood hazard mapping. Hydrol Process 28:4067–4077. doi: 10.1002/hyp.9947

Bates PD, Dawson RJ, Hall JW, et al (2005) Simplified two-dimensional numerical modelling of coastal flooding and example applications. Coast Eng 52:793–810. doi: http://dx.doi.org/10.1016/j.coastaleng.2005.06.001

Bates PD, Horritt MS, Fewtrell TJ (2010) A simple inertial formulation of the shallow water equations for efficient two-dimensional flood inundation modelling. J Hydrol 387:33–45. doi: http://dx.doi.org/10.1016/j.jhydrol.2010.03.027

Baugh CA, Bates PD, Schumann G, Trigg MA (2013) SRTM vegetation removal and hydrodynamic modeling accuracy. Water Resour Res 49:5276–5289.

Bertin X, Li K, Roland A, et al (2014) A modeling-based analysis of the flooding associated with Xynthia, central Bay of Biscay. Coast Eng 94:80–89.

Bontemps S, Defourny P, Bogaert E, et al (2011) GLOBCOVER 2009 - Products Description and Validation Report.

Brakenridge GR, Syvitski JPM, Overeem I, et al (2013) Global mapping of storm surges and the assessment of coastal vulnerability. Nat hazards 66:1295–1312.

Breilh JF, Chaumillon E, Bertin X, Gravelle M (2013) Assessment of static flood modeling techniques: application to contrasting marshes flooded during Xynthia (western France). Nat Hazards Earth Syst Sci 13:1595–1612.

Chadenas C, Creach A, Mercier D (2013) The impact of storm Xynthia in 2010 on coastal flood prevention policy in France. J Coast Conserv 1–10.

Cid A, Castanedo S, Abascal AJ, et al (2014) A high resolution hindcast of the meteorological sea level component for Southern Europe: the GOS dataset. Clim Dyn 1–18.

Condon AJ, Sheng YP (2012) Evaluation of coastal inundation hazard for present and future climates. Nat hazards 62:345–373.

Coulthard TJ, Neal JC, Bates PD, et al (2013) Integrating the LISFLOOD-FP 2D hydrodynamic model with the CAESAR model: implications for modelling landscape evolution. Earth Surf Process Landforms 38:1897–1906. doi: 10.1002/esp.3478

Curtis KJ, Schneider A (2011) Understanding the demographic implications of climate change: estimates of localized population predictions under future scenarios of sea-level rise. Popul Environ 33:28–54.

Dasgupta S, Laplante B, Murray S, Wheeler D (2011) Exposure of developing countries to sea-level rise and storm surges. Clim Change 106:567–579.

DDTM-17 (2011) Éléments de mémoire sur la tempête Xynthia du 27 et 28 février 2010. http://www.charente-maritime.gouv.fr/Politiques-publiques/Environnement-risques-naturels-et-technologiques/Risques-naturels-et-technologiques/Generalites-sur-la-prevention-des-risques-naturels/Elements-de-memoire-Xynthia/Elements-de-memoire-sur-la-tempete-Xynthia-du-27-et-28-fevrier-2010.

De Almeida GAM, Bates P, Freer JE, Souvignet M (2012) Improving the stability of a simple formulation of the shallow water equations for 2-D flood modeling. Water Resour Res 48:n/a–n/a. doi: 10.1029/2011WR011570

Dietrich JC, Zijlema M, Westerink JJ, et al (2011) Modeling hurricane waves and storm surge using integrally-coupled, scalable computations. Coast Eng 58:45–65.

Emanuel KA (2013) Downscaling CMIP5 climate models shows increased tropical cyclone activity over the 21st century. Proc Natl Acad Sci 110:12219–12224. doi: 10.1073/pnas.1301293110

European Environmental Agency (2006) Corine Land Cover 2006. http://www.eea.europa.eu/data-and-maps/data/ds_resolveuid/a47ee0d3248146908f72a8fde9939d9d. Accessed 20 May 2005

European Forum for Geography and Statistics (2009) Estimations carroyées de population Version 2. Gridded fiscal population 2009,.

Forbes C, Luettich Jr RA, Mattocks CA, Westerink JJ (2010) A retrospective evaluation of the storm surge produced by Hurricane Gustav (2008): Forecast and hindcast results. Weather Forecast 25:1577–1602.

Forbes C, Rhome J, Mattocks C, Taylor A (2014) Predicting the Storm Surge Threat of Hurricane Sandy with the National Weather Service SLOSH Model. J Mar Sci Eng 2:437–476.

Fritz HM, Blount CD, Thwin S, et al (2009) Cyclone Nargis storm surge in Myanmar. Nat Geosci 2:448–449.

Gaughan AE, Stevens FR, Linard C, et al (2013) High Resolution Population Distribution Maps for Southeast Asia in 2010 and 2015. PLoS One 8:e55882. doi: 10.1371/journal.pone.0055882

Gedan KB, Kirwan ML, Wolanski E, et al (2011) The present and future role of coastal wetland vegetation in protecting shorelines: answering recent challenges to the paradigm. Clim Change 106:7–29.

Genovese E, Przyluski V (2013) Storm surge disaster risk management: the Xynthia case study in France. J Risk Res 16:825–841.

Grinsted A, Moore JC, Jevrejeva S (2013) Projected Atlantic hurricane surge threat from rising temperatures. Proc Natl Acad Sci 110:5369–5373. doi: 10.1073/pnas.1209980110

Haklay M, Weber P (2008) Openstreetmap: User-generated street maps. Pervasive Comput IEEE 7:12–18.

Hinkel J, Nicholls RJ, Vafeidis AT, et al (2010) Assessing risk of and adaptation to sea-level rise in the European Union: an application of DIVA. Mitig Adapt Strateg Glob Chang 15:703–719.

Hunter NM, Bates PD, Horritt MS, Wilson MD (2007) Simple spatially-distributed models for predicting flood inundation: A review. Geomorphology 90:208–225. doi: http://dx.doi.org/10.1016/j.geomorph.2006.10.021

Jarvis A, Reuter HI, Nelson A, Guevara E (2008) Hole-filled seamless SRTM data V4. Int. Cent. Trop. Agric.

Jongman B, Ward PJ, Aerts JCJH (2012) Global exposure to river and coastal flooding: Long term trends and changes. Glob Environ Chang 22:823–835.

Larsen L, Thomas C, Eppinga M, Coulthard T (2014) Exploratory Modeling: Extracting Causality From Complexity. Eos, Trans Am Geophys Union 95:285–286. doi: 10.1002/2014EO320001

Lewis M, Bates P, Horsburgh K, et al (2013) A storm surge inundation model of the northern Bay of Bengal using publicly available data. Q J R Meteorol Soc 139:358–369. doi: 10.1002/qj.2040

Lewis M, Horsburgh K, Bates P, Smith R (2011) Quantifying the uncertainty in future coastal flood risk estimates for the UK. J Coast Res 27:870–881.

Lloyd S, Kovats RS, Chalabi Z, et al (2015) Modelling the influences of climate change-associated sea-level rise and socioeconomic development on future storm surge mortality. Clim Change 1–15. doi: 10.1007/s10584-015-1376-4

Marcos M, Jordà G, Gomis D, Pérez B (2011) Changes in storm surges in southern Europe from a regional model under climate change scenarios. Glob Planet Change 77:116–128.

McCallum BE, Wicklein SM, Reiser RG, et al (2013) Monitoring storm tide and flooding from hurricane Sandy along the Atlantic coast of the United States, October 2012. 42.

McGranahan G, Balk D, Anderson B (2007) The rising tide: assessing the risks of climate change and human settlements in low elevation coastal zones. Environ Urban 19:17–37.

McMillan HK, Brasington J (2007) Reduced complexity strategies for modelling urban floodplain inundation. Geomorphology 90:226–243.

Mokrech M, Kebede AS, Nicholls RJ, et al (2014) An integrated approach for assessing flood impacts due to future climate and socio-economic conditions and the scope of adaptation in Europe. Clim Change 1–16.

Neumann B, Vafeidis AT, Zimmermann J, Nicholls RJ (2015) Future coastal population growth and exposure to sea-level rise and coastal flooding-A global assessment. PLoS One 10:e0118571.

Nicholls RJ (2003) An expert assessment of storm surge “hotspots.” Interim Re

Quinn N, Lewis M, Wadey MP, Haigh ID (2014) Assessing the temporal variability in extreme storm-tide time series for coastal flood risk assessment. J Geophys Res Ocean 119:4983–4998. doi: 10.1002/2014JC010197

Rappaport EN (2014) Fatalities in the United States from Atlantic tropical cyclones: New data and interpretation. Bull Am Meteorol Soc 95:341–346.

Report MW (2013) Deaths associated with hurricane Sandy - October-November 2012. MMWR Morb Mortal Wkly Rep 62:393–7.

Saito K, Kuroda T, Kunii M, Kohno N (2010) Numerical simulation of Myanmar cyclone Nargis and the associated storm surge part II: Ensemble prediction. 気象集誌 第 2 輯 88:547–570.

Savage JTS, Bates P, Freer J, et al (2015) When does spatial resolution become spurious in probabilistic flood inundation predictions? Hydrol Process n/a–n/a. doi: 10.1002/hyp.10749

Sayama T, Myo Lin N, Fukami K, et al (2012) Storm surge inundation simulation of cyclone Nargis with a rainfall-runoff-inundation model. J. Japan Soc. Civ. Eng. Ser. B1 67:

Schumann GJ-P, Andreadis KM, Bates PD (2014) Downscaling coarse grid hydrodynamic model simulations over large domains. J Hydrol 508:289–298.

Simard M, Pinto N, Fisher JB, Baccini A (2011) Mapping forest canopy height globally with spaceborne lidar. J. Geophys. Res. Biogeosciences 116:

Skinner CJ, Coulthard TJ, Parsons DR, et al (2015) Simulating tidal and storm surge hydraulics with a simple 2D inertia based model, in the Humber Estuary, U.K. Estuar Coast Shelf Sci -. doi: http://dx.doi.org/10.1016/j.ecss.2015.01.019

Smith AB, Katz RW (2013) US billion-dollar weather and climate disasters: data sources, trends, accuracy and biases. Nat hazards 67:387–410.

Smith RAE, Bates PD, Hayes C (2012) Evaluation of a coastal flood inundation model using hard and soft data. Environ Model Softw 30:35–46. doi: http://dx.doi.org/10.1016/j.envsoft.2011.11.008

Stephens EM, Bates PD, Freer JE, Mason DC (2012) The impact of uncertainty in satellite data on the assessment of flood inundation models. J Hydrol 414:162–173.

Stocker TF, Qin D, Plattner G-K, et al (2013) Climate change 2013: The physical science basis. Intergov. Panel Clim. Chang. Work. Gr. I Contrib. to IPCC Fifth Assess. Rep. (AR5)(Cambridge Univ Press. New York)

Torresan S, Critto A, Rizzi J, Marcomini A (2012) Assessment of coastal vulnerability to climate change hazards at the regional scale: the case study of the North Adriatic Sea. Nat Hazards Earth Syst Sci 12:2347–2368.

U.S. Census Bureau (2010) Population & Housing Unit Counts — Blocks.

UNOSAT (2008) Flood assesment for cyclone Nargis affected Ayeyarwady division, Myanmar. http://www.unitar.org/unosat/.

Weatherall P, Marks KM, Jakobsson M, et al (2015) A new digital bathymetric model of the world's oceans. Earth Sp Sci 2:331–345. doi: 10.1002/2015EA000107

Wilson M, Bates P, Alsdorf D, et al (2007) Modeling large-scale inundation of Amazonian seasonally flooded wetlands. Geophys Res Lett 34:n/a–n/a. doi: 10.1029/2007GL030156

Yu D, Lane SN (2006) Urban fluvial flood modelling using a two-dimensional diffusion-wave treatment, part 2: development of a sub-grid-scale treatment. Hydrol Process 20:1567–1583.

Zervas C (2013) Extreme water levels of the United States 1893--2010 NOAA Technical Report NOS CO-OPS 067.

Table 1. Test site physical characteristics, storm tide event properties and socioeconomic impact of flooding.

	Physical Characteristics						Storm Tide			Flood Impact	
test site	coast (km)	area (km^2)	tidal range (m)	land cover (%) urban	land cover (%) crop	land cover (%) forest	name	return period (yr)	max height (m)	deaths	damage (billion USD)
France	100	3570	6	0.4	45.0	3.7	Xynthia	100[a]	4.1	41[c]	3.2[f]
USA	140	7692	2.5	11.3	0.4	45.7	Sandy	500[b]	3.5	53[d]	68[g]
Myanmar	210	12754	3	0.0	53.2	13.7	Nargis	—	6.9	138000[e]	10[e]

[a](Breilh et al 2013)
[b](Aerts et al 2013)
[c](Chadenas et al 2013)
[d](Report 2013)
[e](Fritz et al 2009)
[f](Genovese and Przyluski 2013)
[g](Forbes et al 2014)

Table 2. Percentage of high water marks (HWM) flooded and the vertical error in water heights for each site using dynamic and static models.

test site	dynamic		static	
	HWM flooded (%)	vertical error (RMSE, m)	HWM flooded (%)	vertical error (RMSE, m)
France	62	0.81	65	0.85
USA	32	0.94	32	0.86
Myanmar	40	2.01	52	2.97

Table 3. Observed flood extent, and areas correctly estimated, overestimated, and underestimated using dynamic and static models.

test site	observed	dynamic				static			
	flood area (km^2)	flood area (km^2)	correct (%)	over (%)	under (%)	flood area (km^2)	correct (%)	over (%)	under (%)
France	444	611	79	59	21	1327	95	204	5
USA	553	328	51	8	49	371	57	10	42
Myanmar	4219	4139	65	33	35	8096	92	99	8

Table 4. Population, roads, and agriculture in the observed, dynamic and static flood extents.

test Site	population (counts)			roads (km)			agriculture (km^2)		
	obs.	dynamic	static	obs.	dynamic	static	obs.	dynamic	static
France	19,576	21,721	49,024	1326	1427	2845	282	432	1096
USA	228,825	40,926	56,915	4651	2135	2540	–	–	–
Myanmar	390,115	374,958	880,758	259	266	557	3776	3421	7043

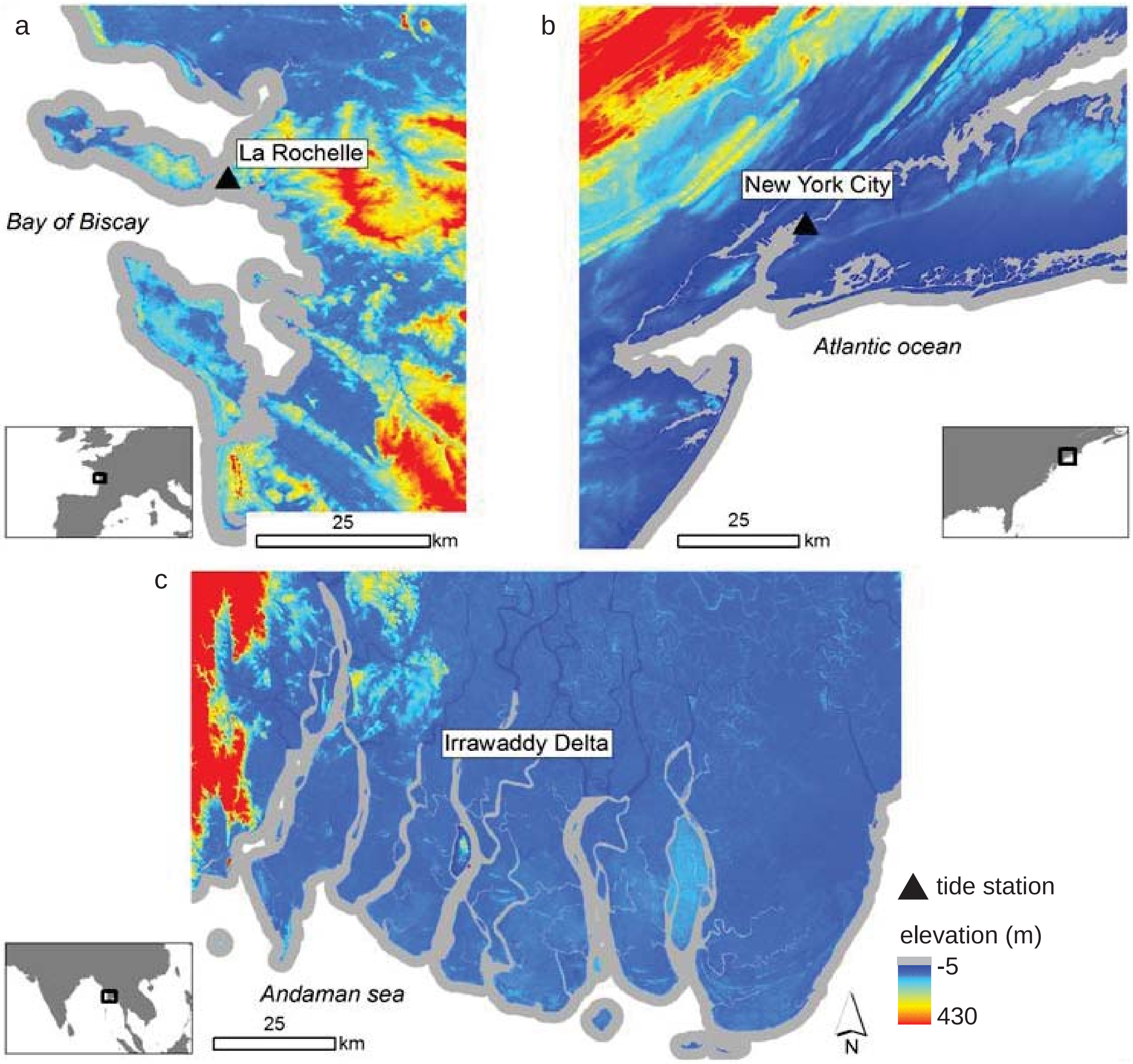

Figure 1. Digital elevation model for sites in (a) west France, (b) north east USA, and (c) south Myanmar.

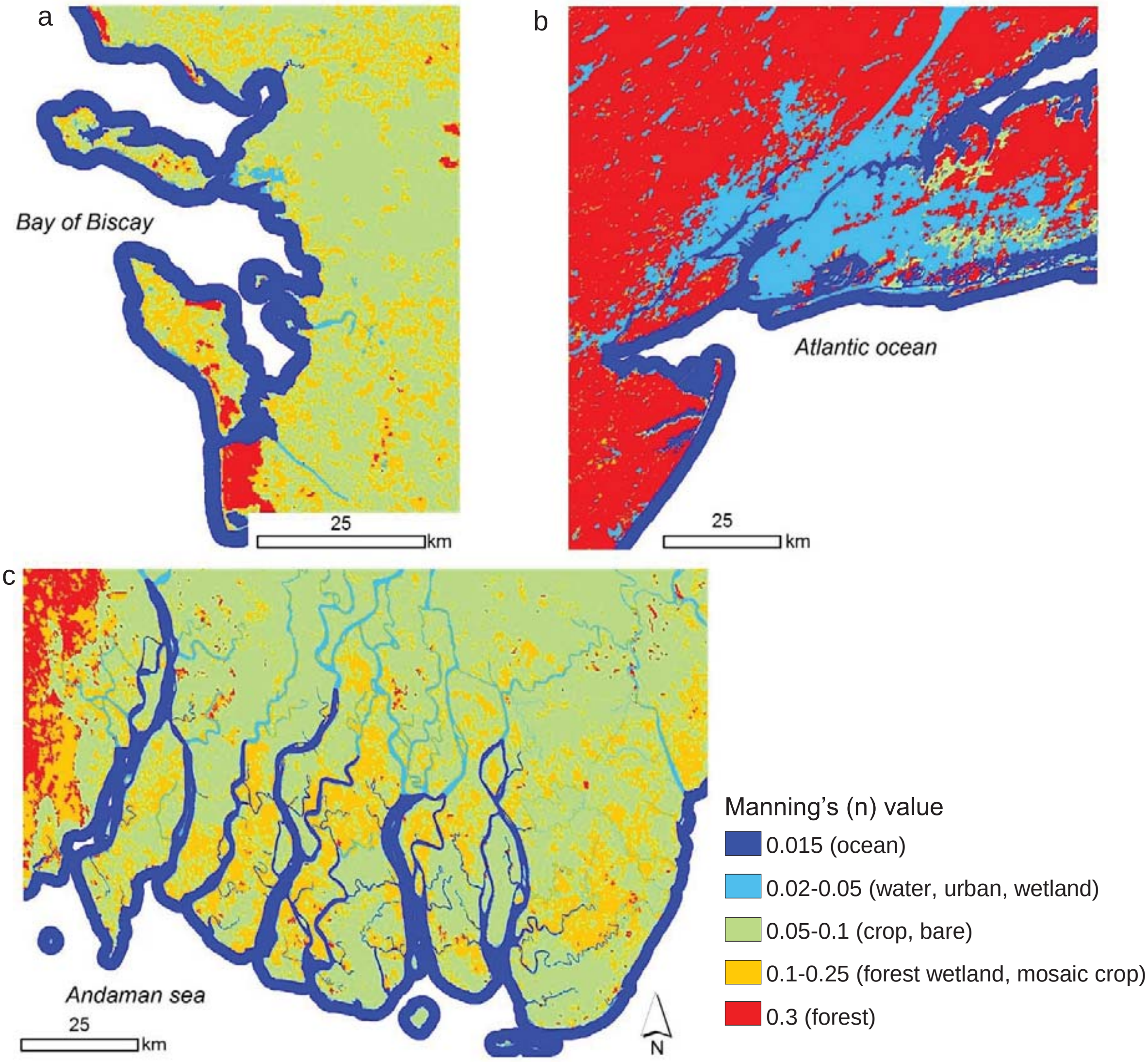

Figure 2. Manning roughness coefficient values (n) for land cover in (a) France, (b) USA, and (c) Myanmar.

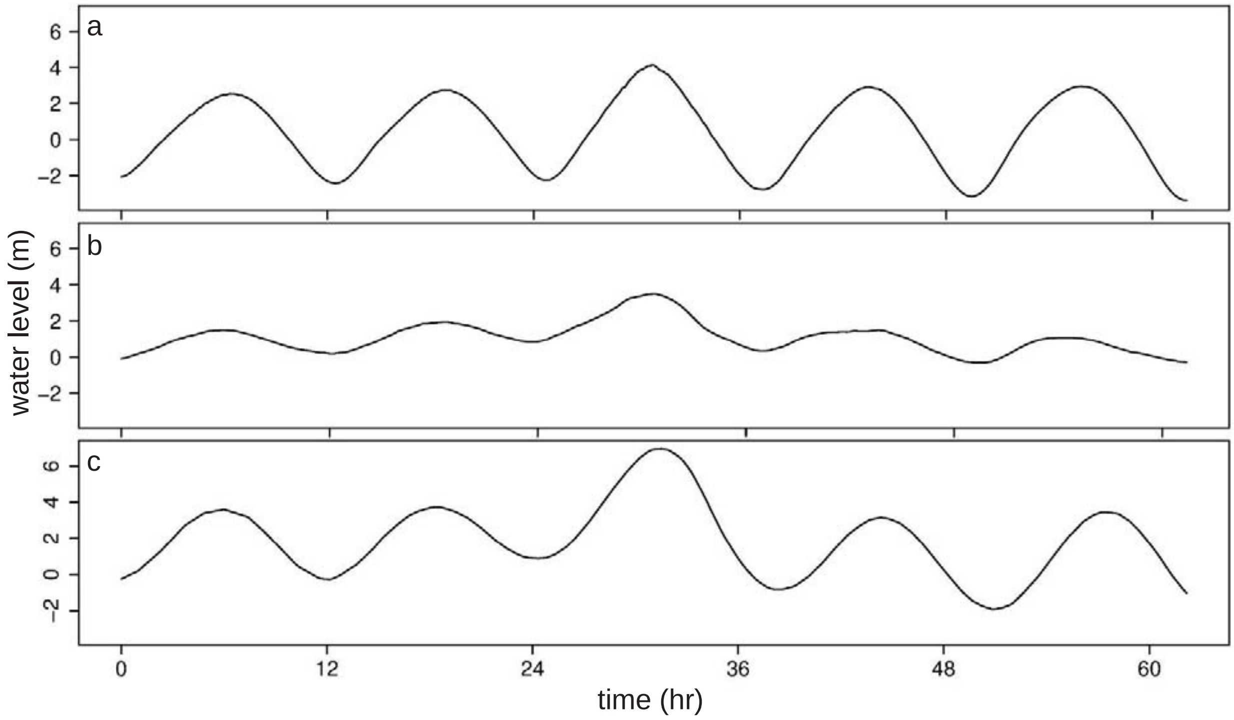

Figure 3. Observed storm tide water levels at tide station (a) La Pallice, France for wind storm Xynthia, (b) The Battery, USA for hurricane Sandy, and (c) simulated water levels for south Myanmar during cyclone Nargis.

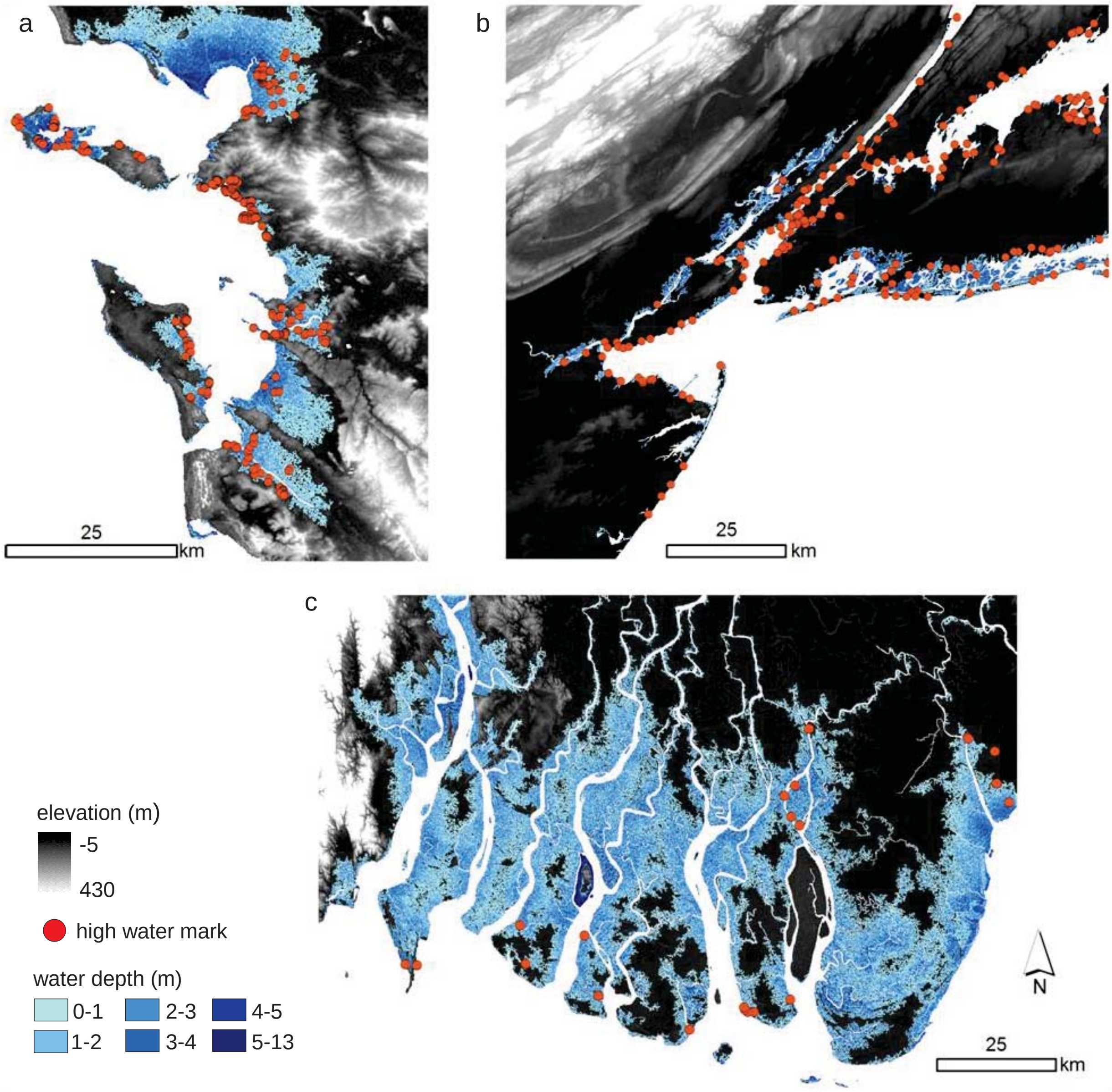

Figure 4. Dynamically modelled maximum water depths and observed high water mark locations for sites in (a) France, (b) USA, and (c) Myanmar.

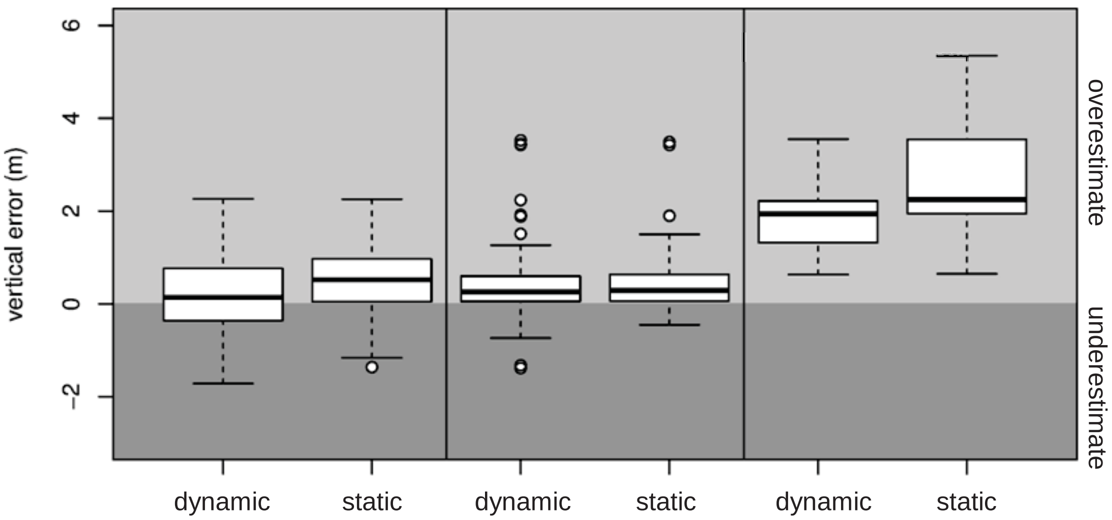

Figure 5. Vertical error between observed high water marks and estimated water heights for dynamic and static models. Vertical error values < 0 m are model water height overestimations and > 0 m model water height underestimations. The interquartile distance (IQD) is the difference between the upper and lower quartiles, and is the central box in the boxplot. Boxplot whiskers extend to upper quartile plus 1.5 times the IQD, and the lower quartile minus 1.5 times the IQD. Open circles represent extreme data values.

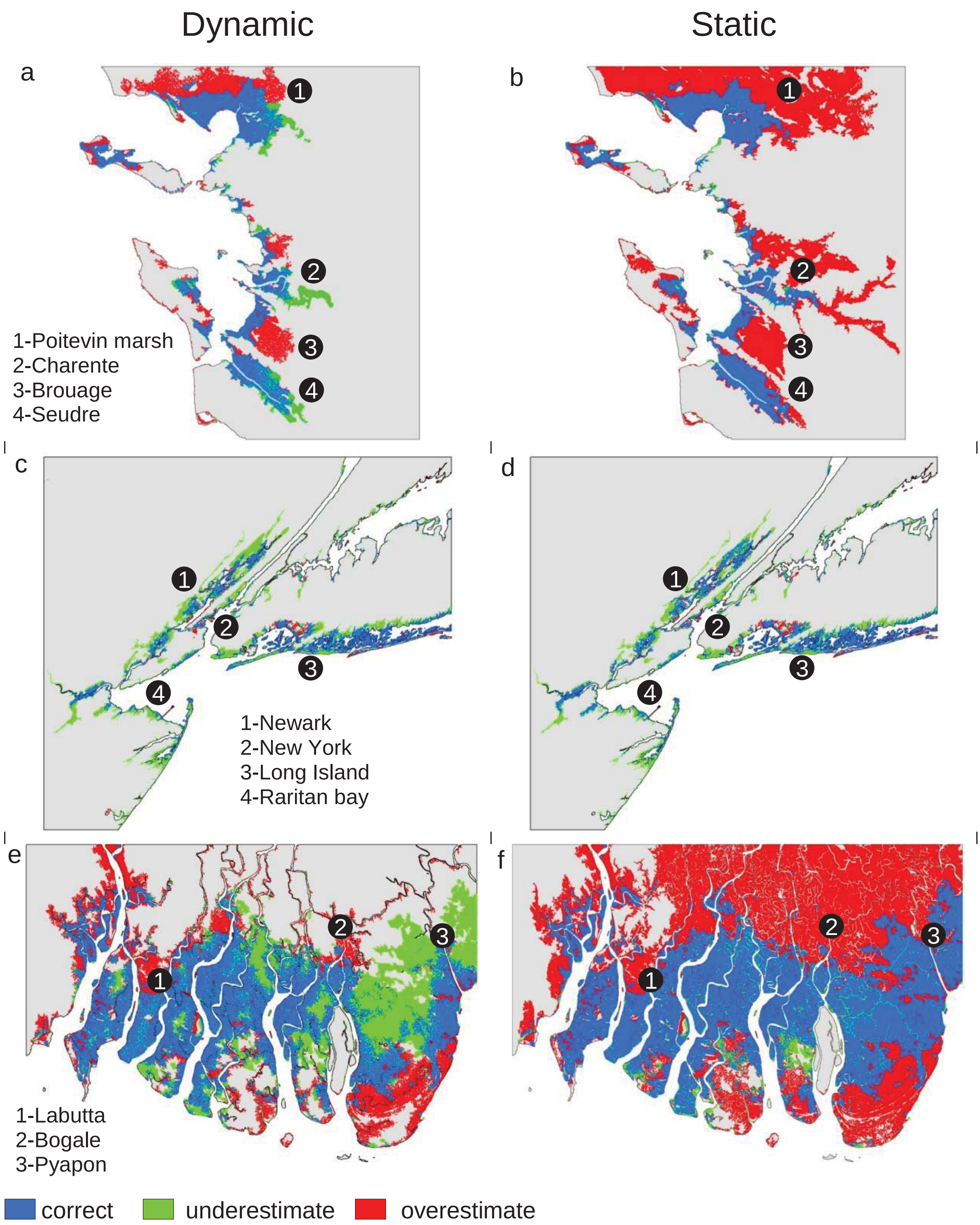

Figure 6. Locations correctly estimated, underestimated, and overestimated using dynamic (left column) and static (right column) models for sites in (a,b) France, (c,d) USA, and (e,f) Myanmar (different horizontal map scale between sites).